

Physicochemical and Antibacterial Characterization of a Novel Fluorapatite Coating

Ahmed Alhilou,^{†,‡} Thuy Do,[‡] Laith Mizban,[†] Brian H. Clarkson,[§] David J. Wood,^{*,†} and Maria G. Katsikogianni^{*,†,||}

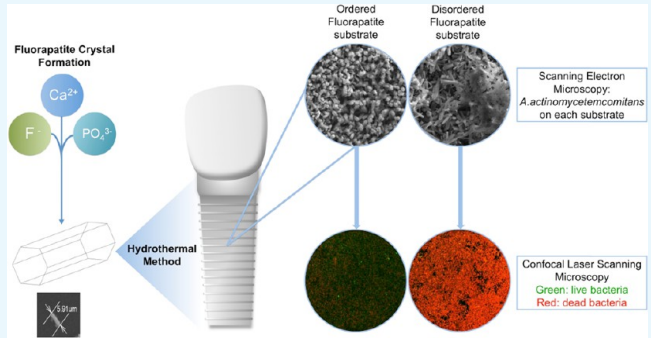
[†]Biomaterials and Tissue Engineering Research Group and [‡]Microbiology and Cell Biology Research Group, School of Dentistry, University of Leeds, Clarendon Way, Leeds LS2 9LU, West Yorkshire, U.K.

[§]Cariology, Restorative Sciences, and Endodontics, School of Dentistry, University of Michigan, Ann Arbor 48109-1078, United States

^{||}Advanced Materials Engineering, Faculty of Engineering and Informatics, University of Bradford, Bradford BD7 1DP, U.K.

S Supporting Information

ABSTRACT: Peri-implantitis remains the major impediment to the long-term use of dental implants. With increasing concern over the growth in antibiotic resistance, there is considerable interest in the preparation of antimicrobial dental implant coatings that also induce osseointegration. One such potential coating material is fluorapatite (FA). The aim of this study was to relate the antibacterial effectiveness of FA coatings against pathogens implicated in peri-implantitis to the physicochemical properties of the coating. Ordered and disordered FA coatings were produced on the under and upper surfaces of stainless steel (SS) discs, respectively, using a hydrothermal method. Surface charge, surface roughness, wettability, and fluoride release were measured for each coating. Surface chemistry was assessed using X-ray photoelectron spectroscopy and FA crystallinity using X-ray diffraction. Antibacterial activity against periodontopathogens was assessed in vitro using viable counts, confocal microscopy, and scanning electron microscopy (SEM). SEM showed that the hydrothermal method produced FA coatings that were predominately aligned perpendicular to the SS substrate or disordered FA coatings consisting of randomly aligned rodlike crystals. Both FA coatings significantly reduced the growth of all examined bacterial strains in comparison to the control. The FA coatings, especially the disordered ones, presented significantly lower charge, greater roughness, and higher area when compared to the control, enhancing bacteria–material interactions and therefore bacterial deactivation by fluoride ions. The ordered FA layer reduced not only bacterial viability but adhesion too. The ordered FA crystals produced as a potential novel implant coating showed significant antibacterial activity against bacteria implicated in peri-implantitis, which could be explained by a detailed understanding of their physicochemical properties.



1. INTRODUCTION

Tooth loss is a significant event that can have a detrimental impact on an individual's well-being and social life. Osseointegrated dental implants are an increasingly viable and successful treatment option for restoring edentulous spaces, demonstrating success rates of up to 96.8%.^{1–3} Worldwide, it is estimated that one million endosseous dental implants are placed per year and around 110 manufacturers produce over 440 implant brands.⁴

It should be noted, however, that clinical complications or failures do occur, and this poses a challenge to both the clinician, in terms of management, and the patient. Implant failure refers to the disruption between the mineralized bone and the implant. The causative factors include chronic bacterial infection known as peri-implantitis, which is defined as “an inflammatory reaction in the oral cavity with loss of supporting

bone in the tissues surrounding an implant.”^{5,6} Recent data have shown that peri-implantitis affects 20% of patients and 10% of implant sites,⁷ making it a serious challenge in long-term implant dentistry. This condition that causes progressive bone loss could eventually lead to severe disfigurement and poor aesthetics, which is extremely challenging to manage and treat.⁸

Bacterial adhesion and biofilm formation on the implant surface are the essential initial steps in the pathogenesis of peri-implant disease and the primary etiological factor of implant failure.⁹ Various anaerobic bacteria, including *Porphyromonas gingivalis* (*P. gingivalis*), *Fusobacterium nucleatum* (*F. nucleatum*),

Received: June 16, 2016

Accepted: August 1, 2016

Published: August 26, 2016

and *Aggregatibacter actinomycetemcomitans* (*A. actinomycetemcomitans*), have been shown to be implicated in peri-implantitis.^{10,11} Because of the growing development of bacterial resistance to antibiotics, there is a considerable interest in the preparation of antimicrobial materials.¹² Therefore, there is great interest in developing an antimicrobial biomimetic implant surface that could prevent bacterial colonization from the outset.

Bioceramics and metals have been of particular interest to researchers. Hydroxyapatite (HA) has long been investigated and, as a result, is the most widely used bioceramic in medicine and dentistry because of its strong affinity to bone tissue. This property improves the implant–bone interface and thus favors early osseointegration.^{13–15} HA, however, does not possess antimicrobial properties, and its use has declined after reports of HA coating delamination from oral implants, resulting in poor performance and uncertain long-term success.¹⁶

As a result of these limitations, fluoride-containing apatite coatings have become an area of interest. Chen et al. (2006) successfully synthesized fluorapatite (FA) crystals that resembled enamel prismlike structures, using the hydrothermal technique. The advantage of these FA microrods is that their composition is similar to the apatite crystals found in dental hard tissues.¹⁷

FA demonstrates better biocompatibility and bioactivity when compared with HA.^{18–20} This bioceramic also exhibits lower resorption rates in situ²¹ and has the potential to release fluoride ions, which have osteoinductive²² and antibacterial properties.²³ Indeed, FA has been shown to improve the rate of bone apposition in early osteogenesis.²⁴ These promising findings suggest that FA implant coatings may be clinically advantageous and have led to an increased interest in the application of FA as a dental implant coating. However, current research regarding this material is not comprehensive.²⁵ For instance, there are controversies as to whether partially fluorine-substituted hydroxyapatite (FHA; $\text{Ca}_{10}(\text{PO}_4)_6(\text{OH})_{2-2x}\text{F}_{2x}$, $0 < x < 1$) possesses significant antimicrobial activity over HA, especially when different bacterial species are compared,^{26–28} whereas the antimicrobial efficacy of FA is largely unreported. Given the well-documented issues of peri-implantitis, it would be beneficial to ascertain whether an FA coating exhibits antimicrobial activity in addition to its osteoinductive properties. In this direction, the aim of this study was to investigate the potential antibacterial effects of FA dental implant coatings. The null hypothesis tested was that there would be no difference in microbial response between the coated and control stainless steel (SS) substrates.

2. MATERIALS AND METHODS

2.1. Production of Ordered and Disordered FA Coatings. Grade 430 SS alloy discs, 14 mm in diameter and 0.5 mm in thickness, with smooth edges and flat surface (Ted Pella Inc, Redding, CA, USA) were used as substrates to grow FA crystals using the hydrothermal method¹⁷ as reported previously. Prior to the growth of FA crystals, the SS discs were acid-etched with piranha solution [1:1 sulphuric acid (98%)/hydrogen peroxide (30%)] for 24 h and then rinsed copiously with distilled water.

For the synthesis of FA crystals, 9.36 g of ethylene diamine tetraacetic acid calcium disodium salt (EDTA-Ca-Na₂) and 2.07 g of NaH₂PO₄·H₂O were mixed with 90 mL of distilled water. The suspension was stirred continuously until the powder dissolved. The pH was adjusted to 6.0 using NaOH. Finally,

0.21 g of NaF dissolved in 10 mL of water (pH 7.0) was added under continuous stirring to 90 mL of the EDTA-Ca-Na₂ and NaH₂PO₄ solution.

FA crystal growth was achieved by placing the SS discs in 100 mL of a newly prepared EDTA-Ca-Na₂/NaH₂PO₄/NaF mixture and then autoclaving at 121 °C under a pressure of 2.4×10^5 Pa for 10 h. The ordered and disordered FA coatings were produced individually on the under and upper surfaces of the SS discs, respectively. The exact mechanism of crystal formation and self-assembly has been extensively described by Chen et al.¹⁷

2.2. Material Characterization. **2.2.1. Scanning Electron Microscopy (SEM) and Energy Dispersive Spectroscopy.** SEM was used to examine the surface topography of the bare SS discs and the discs coated with ordered and disordered FA crystals. The samples were prepared by attaching them to aluminum stubs using carbon tabs; they were then examined using a Hitachi S-3400N variable pressure scanning electron microscope under low vacuum at 20 kV, and images were generated using a back-scattered electron detector. An X-ray energy dispersive spectrometer (Bruker 4030 Quantax SDD-EDS System) equipped with the scanning electron microscope was used for the elemental analysis of the FA coatings. The 20 kV accelerating voltage that was used allowed for the elemental analysis of the first micron of the surface and the evaluation of the surface fluorine content of each of the FA coatings. Moreover, a map was produced using specific elements, for example, calcium and fluorine for the coatings and chromium for the SS substrate, and overlaid on the corresponding SEM image. In parallel, a line scan was produced across a scratch made on the surface of the coatings, using a scalpel. These allowed for the observation of the elemental distribution over an area and over the coating depth.

2.2.2. X-ray Photoelectron Spectroscopy. The surface chemical composition of bare and FA-coated SS discs was determined using X-ray photoelectron spectroscopy (XPS) at the National EPSRC XPS Users Service (NEXUS) at Newcastle University, an EPSRC mid-range facility. XPS data were obtained with an AXIS Nova spectrometer (Kratos Analytical) using a high-power monochromated Al K α X-ray source. The survey spectra were acquired, and CasaXPS (Casa Software Ltd) data analysis software was used to calculate the elemental compositions.

2.2.3. Fluoride Release Measurements. The concentration of the fluoride ions released into the culture media along with the media pH was determined by collecting the supernatant of each cultured sample, as detailed in section 2.3, after 48 h of incubation and analyzing it using an Orion 920A fluoride electron (Orion Research Inc.), following the manufacturer's instructions. Briefly, fluoride standards of 0.1, 1, 10, and 100 mg/L (ppm F) were measured in triplicate and used to construct a calibration curve. The supernatant of three independently prepared substrates was treated with an equal volume of total ionic strength adjustment buffer (TISAB) and measured in triplicate. The fluoride concentrations in the unknown samples were evaluated using the calibration curve.

2.2.4. 3D Optical Profiler. The surface morphology, roughness, area, and thickness of the ordered and disordered FA coatings on the SS discs were evaluated using a white light interferometric three-dimensional (3D) optical profilometer (Bruker, NPFLEX) operating in the vertical scanning interferometry (VSI) mode. The instrument calculates (1) the average surface roughness (S_a), which is the arithmetic

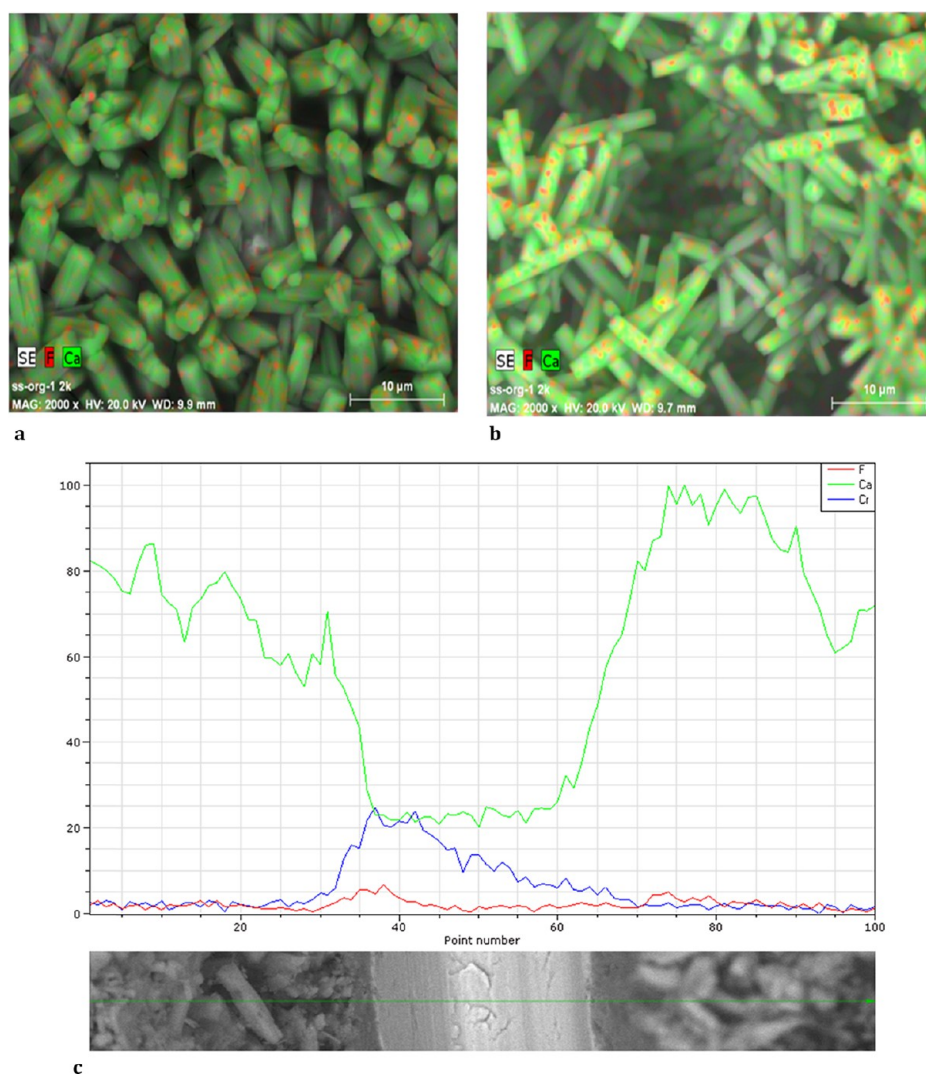


Figure 1. (a) EDS map of the ordered FA coating on the SS discs, (b) EDS map of the disordered FA coating on the SS discs, and (c) line scan profile of a cut made with a scalpel blade in a disordered FA coating on the SS discs.

mean of peaks and valleys or departures from the centerline over the sampling length; (2) the root mean square roughness (S_q), which is the root mean square measurement of the peaks and valleys or departures from the centerline; and (3) the maximum distance between the highest peak and the lowest groove (S_z). The analysis of the variation of the coating thickness enabled the estimation of an average thickness value over the scanned surface, at an instrumental resolution of approximately 5 nm. For the roughness and surface area measurements, an $\times 50$ objective was used, and for thickness measurements, an $\times 2.5$ objective was used. For the statistical evaluation of the morphology parameters, three independently prepared substrates were examined and each measurement was repeated three times on each substrate.

2.2.5. Streaming and Zeta Potential Measurements. The surface charge of bare and ordered or disordered FA-coated SS discs was evaluated in 0.01 M phosphate buffer saline (PBS) using a SurPASS electrokinetic analyser (Antor Paar). In parallel, the zeta potential of the FA crystals after grinding, and of the bacterial strains used, as detailed in section 2.3, was evaluated in both 0.01 M PBS and brain heart infusion (BHI) bacterial culture medium broth (Oxoid), using a laser zeta meter (Malvern).

2.2.6. Water Contact Angle (WCA) Measurements. The surface wettability of the ordered and disordered FA coatings as well as of the SS discs was examined by measuring the WCA using a MicroDrop analyzer (First Ten Angstroms), using the sessile drop technique at room temperature.

2.2.7. X-ray Diffraction (XRD) Analysis. XRD was used to identify the composition of the crystal phases within the FA coatings. The XRD data were obtained using a Philips analytical PW3050 system with a copper $K\alpha$ X-ray source ($\lambda = 1.5418 \text{ \AA}$), 40 kV tension, and 35 mA current. The scans were taken between 20 and 60° , with a step size of 0.05° and dwell of 1 s. The data collected were analyzed using PC-APD diffraction software.

2.3. Antibacterial Tests. The antibacterial properties of the ordered and disordered FA coatings on the SS discs were examined using single species cultures of *Porphyromonas gingivalis* W50 (*P. gingivalis*), *Fusobacterium nucleatum* ATCC 10953 (*F. nucleatum*), and *Aggregatibacter actinomycetemcomitans* NCTC 9710 (*A. actinomycetemcomitans*).

2.3.1. Viable Count. Before testing, the discs (ordered FA, disordered FA, or acid-etched SS) were sterilized in an ultraviolet chamber (Bio-Rad GS Gene Linker UV chamber) at 250 mJ for three consecutive cycles. Starting with an

Table 1. EDS and XPS Analyses of the Various Substrates

sample	Ca/P (EDS)	Ca/F (EDS)	F (wt %) (EDS)	Fe/Cr (EDS)	Ca/F (XPS)	F (at %) (XPS)	F release (ppm in BHI)
SS	N/A	N/A	N/A	5.82 ± 0.05	N/A	N/A	N/A
FA ordered	1.75 ± 0.13	5.36 ± 0.88	2.7 ± 0.3	N/A	7.45 ± 0.38	1.21 ± 0.23	5.1 ± 1.5
FA disordered	1.75 ± 0.10	3.72 ± 0.70	3.4 ± 0.4	N/A	5.84 ± 0.29	1.82 ± 0.29	17.8 ± 1.2

inoculum of 2.5×10^8 bacteria per sample, biofilms were grown on the surface of each disc by incubating them in BHI broth at 37 °C in an anaerobic incubator (Ruskinn concept 1000 Invivo, Ruskinn Technology Ltd) under anaerobic conditions (80% N₂, 10% CO₂, and 10% H₂ atmosphere) for 48 h. The reduced BHI broth (1 mL) was carefully added to each disc sample every 24 h without disturbing the biofilm surface and to maintain biofilm growth. The growth experiments were carried out in triplicate. Each disc was then carefully transferred into 2 mL sterile reduced transport fluid (RTF)²⁹ and vigorously vortexed for 1 min to disrupt the adhered biofilm and homogeneously suspend the bacteria. Serial dilutions were carried out up to 10⁻⁶ in the sterile RTF solution, and then 0.1 mL of the highest dilution (10⁻⁴, 10⁻⁵, and 10⁻⁶) was spread onto blood agar plates (Columbia blood agar base, Oxoid). The plates were incubated at 37 °C for 48 h in an anaerobic incubator, the number of colonies on each agar plate was visually counted using a colony counter (Stuart SC6), and the colony-forming units (CFUs) per milliliter were calculated.

2.3.2. Scanning Electron Microscopy. The biofilm growth experiments were repeated, and each disc was fixed overnight with 2.5% glutaraldehyde in PBS. Afterward, the samples were dehydrated by several passages in ethanol, using increasing concentrations of ethanol up to 100%, sputter coated with gold, and investigated using the Hitachi S-3400N SEM, under low vacuum at 20 kV. Images were generated using a back-scattered electron detector and analyzed in terms of surface coverage using ImageJ software.

2.3.3. Confocal Laser Scanning Microscopy (CLSM). A spectral confocal laser scanning microscope (TCS SPE, Leica, GmbH) and a Live/Dead BacLight bacterial viability kit L7012 (Molecular Probes) were used for the determination of the live/dead ratio of the bacteria attached to the various substrates, 48 h post adhesion. The attached bacteria were stained with a 1:1 SYTO 9 dye, 3.34 mM/propidium iodide 20 mM in 0.85% NaCl. The SYTO 9 stain generally labels all bacteria in a population whereas propidium iodide penetrates bacteria with damaged membrane, thereby staining only the dead bacteria and reducing the SYTO 9 fluorescence when both dyes are present. After staining, the samples were incubated at room temperature in the dark for 15 min and subsequently examined using CLSM. The live/dead ratios were calculated using CLSM software.

2.4. Statistical Analysis. Statistical analysis of the results was performed with Statistical Package for Social Sciences (SPSS); all data were expressed as mean ± standard deviation of the mean. One-way analysis of variance (ANOVA) followed by the Student's *t* test was used to detect the significant differences ($p < 0.05$ was chosen to denote the significance level).

3. RESULTS

3.1. Material Characterization. **3.1.1. SEM and Energy Dispersive Spectroscopy.** SEM images showed that the length of the FA crystals that were prepared using the hydrothermal method was $6 \pm 2 \mu\text{m}$. In the case of the ordered coatings, the

crystals were well-aligned, with the *c*-axis of the crystals arranged perpendicular to the SS substrate, whereas in the case of the disordered coatings, the crystals were randomly oriented.

Shown below are representative energy dispersive spectroscopy (EDS) maps of the ordered FA coating (Figure 1a) and the disordered ones (Figure 1b). The EDS maps are composites of three images: (1) the secondary electron image generated by SEM and (2 and 3) elemental maps of colored pixels corresponding to different elements—calcium represented by green pixels and fluoride represented by red pixels overlaid on the original SEM image. A line scan of calcium, fluoride, and chromium also confirms that fluorine was apparently present on the cut surface of the substrate for a disordered coating (Figure 1c).

The relative fluoride content of each of the three surfaces, SS, ordered and disordered FA coatings, measured using EDS, is shown in Table 1. The highest fluoride content was measured on the disordered coating, and the results were statistically different ($p < 0.05$). Apart from fluoride (F), calcium (Ca), phosphorous (P), and sodium (Na) were detected on the ordered and disordered FA coatings but not on the noncoated SS substrate. Only chromium (Cr) and iron (Fe) were detected on the SS substrate. The presence of carbon (C) and oxygen (O) was confirmed on all three substrates. The Ca/P, Ca/F, Fe/Cr ratios along with the F (wt %) obtained for all substrates using EDS are presented in Table 1.

3.1.2. X-ray Photoelectron Spectroscopy. The chemical compositions of each of the three surfaces (SS, ordered, and disordered FA coatings) were also compared using XPS analysis (Figure 2). Fluoride (F 1s), calcium (Ca 2p), phosphorous (P 2p), and sodium (Na 1s) were detected on the ordered and disordered FA coatings whereas none of these were observed on the noncoated SS substrate. In contrast, chromium (Cr 2p), iron (Fe 2p), and silicon (Si 2p) were detected only on the bare SS surface. Concentrations of other elements, including carbon (C 1s), oxygen (O 1s), and nitrogen (N 1s), were similar on the three surfaces (Table 1). The XPS elemental analysis showed higher atomic concentrations of F 1s, Ca 2p, P 2p, and Na 1s on the disordered FA coating, in comparison to the ordered coating, whereas the Ca/F ratio was lower, as presented in Table 1.

3.1.3. Fluoride Release Measurements. The measurement of the concentration of the fluoride ions that were released into the supernatant of each cultured sample in BHI showed that more fluoride was released in the case of the disordered coating than in the case of the ordered coating (Table 1). The concentration of the fluoride ions that were released was not affected by the presence of the bacterial strains tested in this study [*P. gingivalis* (*P. ging*), *F. nucleatum* (*F. nunc*), and *A. actinomycetemcomitans* (*A. A.*)] and the pH of the suspension when compared with BHI (Table 2).

3.1.4. 3D Optical Profiler—Roughness, Thickness, and Surface Area Measurements. Table 3 illustrates the average surface roughness (S_a), the root mean square roughness (S_q), and the maximum distance between the highest peak and the lowest groove (S_z) of the three surfaces (SS, ordered, and

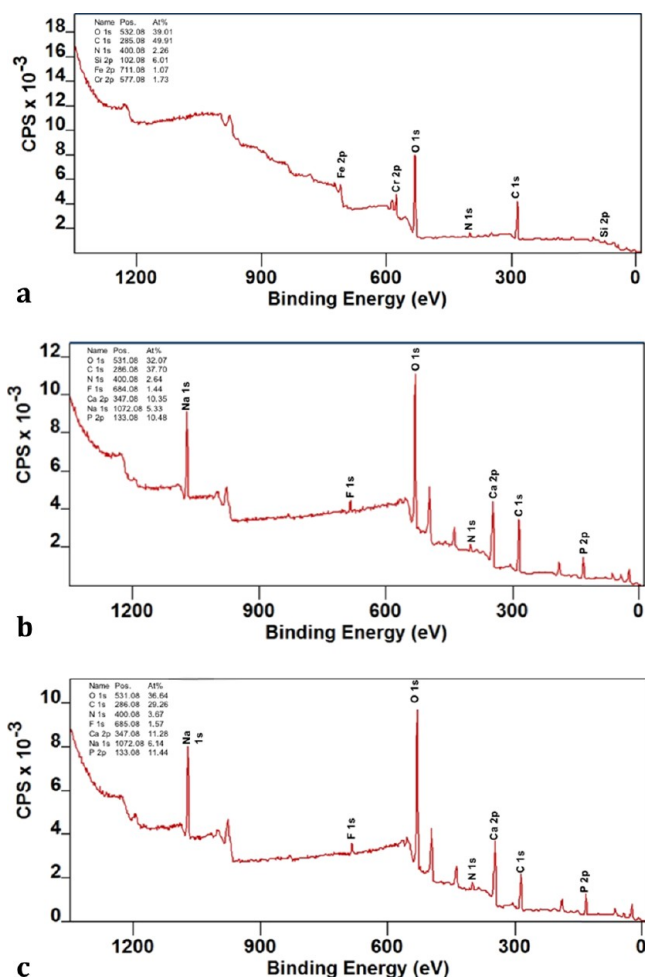


Figure 2. XPS spectra of (a) acid-etched SS, (b) ordered FA coating on SS, and (c) disordered FA coating on SS.

disordered FA coatings). The results (Figure 3 and Table 3) indicate that the roughness values of the disordered FA coating were significantly higher than those of both the ordered FA coating and the SS discs. Nevertheless, the ordered FA coating presented significantly higher roughness values than did the SS discs.

When compared with the ordered coating, the disordered coating was significantly thicker and had a much higher measured surface area, as presented in Table 3. The ordered coating had significantly higher measured surface area in comparison to the bare SS discs.

3.1.5. Streaming and Zeta Potential Measurements. The SPMs illustrated in Table 3 show that the SS surface exhibited a significantly more negative surface charge than those of both FA coatings whereas the disordered FA coating appeared to be neutral. The zeta potential measurements of ground FA powder in 0.01 M PBS and BHI showed that FA appears neutral under these conditions whereas the three tested bacterial strains (*P.*

gingivalis, *F. nucleatum*, and *A. actinomycetemcomitans*) appeared highly negatively charged in 0.01 M PBS, with *F. nucleatum* and *P. gingivalis* being more negatively charged than *A. actinomycetemcomitans* (Table 4). The presence of BHI decreased the bacterial charges, but still *F. nucleatum* and *P. gingivalis* appeared more negatively charged than *A. actinomycetemcomitans* (Table 4).

3.1.6. WCA Measurements. The WCA measurements on the three surfaces showed that SS is moderately hydrophobic, with an average WCA of $45 \pm 2^\circ$, whereas the WCA could not be measured on the FA coatings as the droplets started to spread (Table 3).

3.1.7. X-ray Diffraction. The diffraction patterns of the surfaces are shown in Figure 4. The disordered FA crystals show a diffraction pattern that corresponds to that of the reference diffraction file (top and bottom traces). The diffraction pattern of the ordered FA crystals shows the same peak positions as that of the disordered crystals, confirming it is the same material but with different peak heights, suggesting preferential orientation of the crystals, which was also observed using SEM. This pattern also shows the diffraction peaks associated with the underlying SS substrate, supporting the visual observation that this coating is very thin.

The reference file used for the FA standard was FA reference (04-009-4021) (chemical formula, $\text{Ca}_5(\text{PO}_4)_3\text{F}$; crystal system, hexagonal).

3.2. Antibacterial Tests. The efficacy of the two coatings against bacteria was assessed using the CFUs counting method, SEM, and confocal microscopy.

3.2.1. Viable Count. The results presented in Figure 5, using the viable count method, show that the FA coated substrates (both ordered and disordered) significantly reduced the viability of the adherent bacteria, for all three bacterial strains tested (*P. gingivalis*, *F. nucleatum* and *A. actinomycetemcomitans*), in comparison to the bare SS substrate. In the case of *P. gingivalis*, the disordered FA coating reduced the bacterial viability more than the ordered coating by $89 \pm 2\%$ and $68 \pm 4\%$, respectively, whereas for the other two bacterial strains, *F. nucleatum* and *A. actinomycetemcomitans*, the two FA coatings (ordered and disordered) appeared equally potent in reducing the bacterial viability, 48 h post adhesion. In the case of *F. nucleatum*, the reduction in growth was $84 \pm 12\%$ for the ordered coating and $82 \pm 15\%$ for the disordered coating. In the case of *A. actinomycetemcomitans*, the reduction in growth was $96 \pm 10\%$ for the ordered coating and $90 \pm 12\%$ for the disordered coating.

3.2.2. Scanning Electron Microscopy. The SEM results presented in Figure 6 show, in Column A, that the surface of the bare SS substrate was fully covered by a *P. gingivalis* biofilm 48 h post adhesion whereas the ordered FA coating was partially covered by bacteria, with a $32 \pm 3\%$ coverage. In contrast to the ordered FA coating, the disordered coating was fully covered by a biofilm that was penetrating the porous structure of the disordered coating. This shows a significant difference between the two substrates, ordered and disordered,

Table 2. Culture Media pH and Fluoride Release from the Substrates in BHI and in the Presence of Various Bacterial Strains

sample	BHI pH	A. A. pH	<i>P. ging</i> pH	<i>F. nunc</i> pH	BHI F release (ppm)	A. A. F release (ppm)	<i>P. ging</i> F release (ppm)	<i>F. nunc</i> F release (ppm)
SS	6.6 ± 0.1	5.3 ± 0.1	7.4 ± 0.1	6.8 ± 0.1	N/A	N/A	N/A	N/A
FA ordered	6.6 ± 0.1	5.3 ± 0.1	7.4 ± 0.1	6.8 ± 0.1	5.1 ± 1.5	5.7 ± 1.2	5.2 ± 1.2	5.9 ± 1.6
FA disordered	6.6 ± 0.2	5.4 ± 0.2	7.3 ± 0.1	6.7 ± 0.1	17.8 ± 1.2	18.6 ± 1.4	16.8 ± 1.1	19.2 ± 1.4

Table 3. Roughness Values, Thickness, Measured Surface Area, Streaming Potential Measurement (SPM), and Contact Angle Measurement of Various Substrates

sample	S_a (μm)	S_z (μm)	thickness (μm)	measured surface area (mm^2)	SPM (mV) in 0.01 M PBS	CAM (deg)
SS	0.33 ± 0.06	4.23 ± 0.46	N/A	0.079 ± 0.1	-31.52 ± 3.31	45 ± 2
FA ordered	4.78 ± 1.02	83.35 ± 5.73	7.28 ± 0.46	0.61 ± 0.24	-10.51 ± 3.23	<5
FA disordered	9.63 ± 1.04	106.47 ± 7.72	49.07 ± 6.58	1.51 ± 0.26	0.32 ± 0.52	<5

with the ordered presenting better nonfouling properties than the disordered and the bare SS substrate. Similar results were obtained with the other two bacterial strains (*F. nucleatum* and *A. actinomycetemcomitans*): the ordered FA coating presented better nonfouling properties against these two bacterial strains than did the disordered and the bare SS substrate. In the case of *F. nucleatum* (Figure 6, column B), the surface coverage of the ordered FA substrate was $65 \pm 4\%$ whereas in the case of *A. actinomycetemcomitans* (Figure 6, column C), the coverage was $41 \pm 2\%$, compared with the fully covered FA disordered and the SS substrates.

3.2.3. Confocal Laser Scanning Microscopy. Figure 7 presents some of the images obtained using the confocal laser scanning microscope. The green fluorescent stain represents the live bacteria whereas the red fluorescent stain represents the dead bacteria. As in the case of *P. gingivalis* examined using SEM (Figure 6), CLSM showed that the disordered FA coating was more populated by the *F. nucleatum* biofilm, 48 h post adhesion, than the ordered coating; however, most of the adherent bacteria appeared dead. Comparing the ordered FA coating against the bare SS, CLSM showed that the ordered coating was more potent as antibacterial against *F. nucleatum*, in comparison to the bare SS substrate.

Similar data were obtained for the other two bacteria strains *P. gingivalis* and *A. actinomycetemcomitans*, showing that the disordered FA coating was more effective against the various bacterial strains, but at the same time it was retaining more bacteria in total, in comparison to the ordered one. Quantitative analysis of these data is shown in Figure 8.

4. DISCUSSION

To date, there has been limited research on the antimicrobial properties of viable laboratory-produced FA implant materials. The aim of the present study was to investigate the antibacterial activity of ordered and disordered FA coatings manufactured using the hydrothermal method. The effect that these coatings had on the growth of three putative bacterial strains that are commonly implicated in peri-implant disease was identified.¹⁰ Physicochemical analysis of the FA crystals produced in the current study was carried out to achieve a comprehensive material appraisal.

4.1. Formation of FA Coatings on SS Discs. The hydrothermal method is widely used in nanotechnology to produce long nanorods, nanofibers, and other one-dimensional nanostructures. Chen et al. (2006) and Czajka-jakubowska et al. (2009)^{30,31} showed that this process produces FA crystals that are well-aligned and self-assemble into an ordered enamel prismlike structure. Another way of creating these enamel prismlike analogues involves modifying the surface of a synthetic HA nanorod, using sodium bis(2-ethylhexyl) sulfosuccinate (AOT). However, this method results in prisms that are too small: approximately 400 nm in length and 100 nm in cross section.³⁰ The hydrothermal method can create prisms that are more comparable with enamel nanorod dimensions: 1–3 μm in cross section and 50 μm in length.³⁰ The

hydrothermal method exhibits greater potential as a manufacturing process because it allows control of the nanorod composition and size. Therefore, the present study would further explore this more viable method.

The data gathered in section 3.1 show that, in the case of the ordered FA coating, the FA crystals produced by the hydrothermal method were well-aligned with the *c*-axis and assembled into an ordered enamel prismlike structure perpendicular to the SS substrate. They were 6–8 μm in length and densely packed, giving a 7.28 ± 0.46 μm thick coating. The disordered FA coating comprised of FA crystals arranged in random orientations, giving a 49.07 ± 6.58 μm thick coating.

The XRD characterization of the SS discs, ordered FA coatings and disordered FA coatings can be seen in Figure 3. The graph confirms the apatitic structure of the crystals in the coatings as compared with the FA reference peaks. This confirms that the disordered and ordered FA is crystalline in nature, which is in agreement with the findings of Czajka-jakubowska et al. (2009). It is well known that HA coatings deposited by plasma-spraying contain a mixture of crystalline and amorphous crystalline phases; in contrast, this method produces a phase pure coating. Crystalline structures are more resistant to dissolution,³² which could be clinically advantageous.

Including the present study, a number of authors now cite success in growing FA crystals on SS using the hydrothermal method.^{31,33} Czajka-jakubowska et al. used the same method to deposit FA on titanium, which is the most commonly used material in implant dentistry.³¹ The FA crystals deposited on both titanium and SS have been found to exhibit the same composition, alignment, size, shape, and structure³¹ (Figures S1 and S2, respectively). Therefore, using SS as the substrate throughout this investigation serves a cost-effective, yet still relevant, purpose because it is the coating that is examined rather than the substrate. The ability to grow FA crystal coatings on these metals shows promising signs for commercial use in implant dentistry.

Various forms of fluoride-containing apatites have been found to exhibit osteoinductive properties.^{34,35} This is partly due to the presence of fluoride ions, which increases the proliferation and differentiation of osteoprogenitor cells.²² Improved osteoblast numbers form bone at a faster rate, thus promoting earlier implant osseointegration. An in vivo study performed by Dhert et al. in goats showed that FA implant coatings are superior to HA in favoring osteoinduction.²⁴ FA has also been reported to suppress the maturation of osteoclasts and inhibit phagocyte activity, which may be contributing factors to the biocompatibility these coatings present.³⁶

Liu et al. observed a favorable cellular response in osteoblast-like cells on both ordered and disordered FA coatings in vitro. The same group also demonstrated accelerated and enhanced mineralized tissue formation integrated within ordered FA coatings in vivo. In particular, after 5 weeks, over 80% of the ordered FA coating was integrated with the mineralized tissue

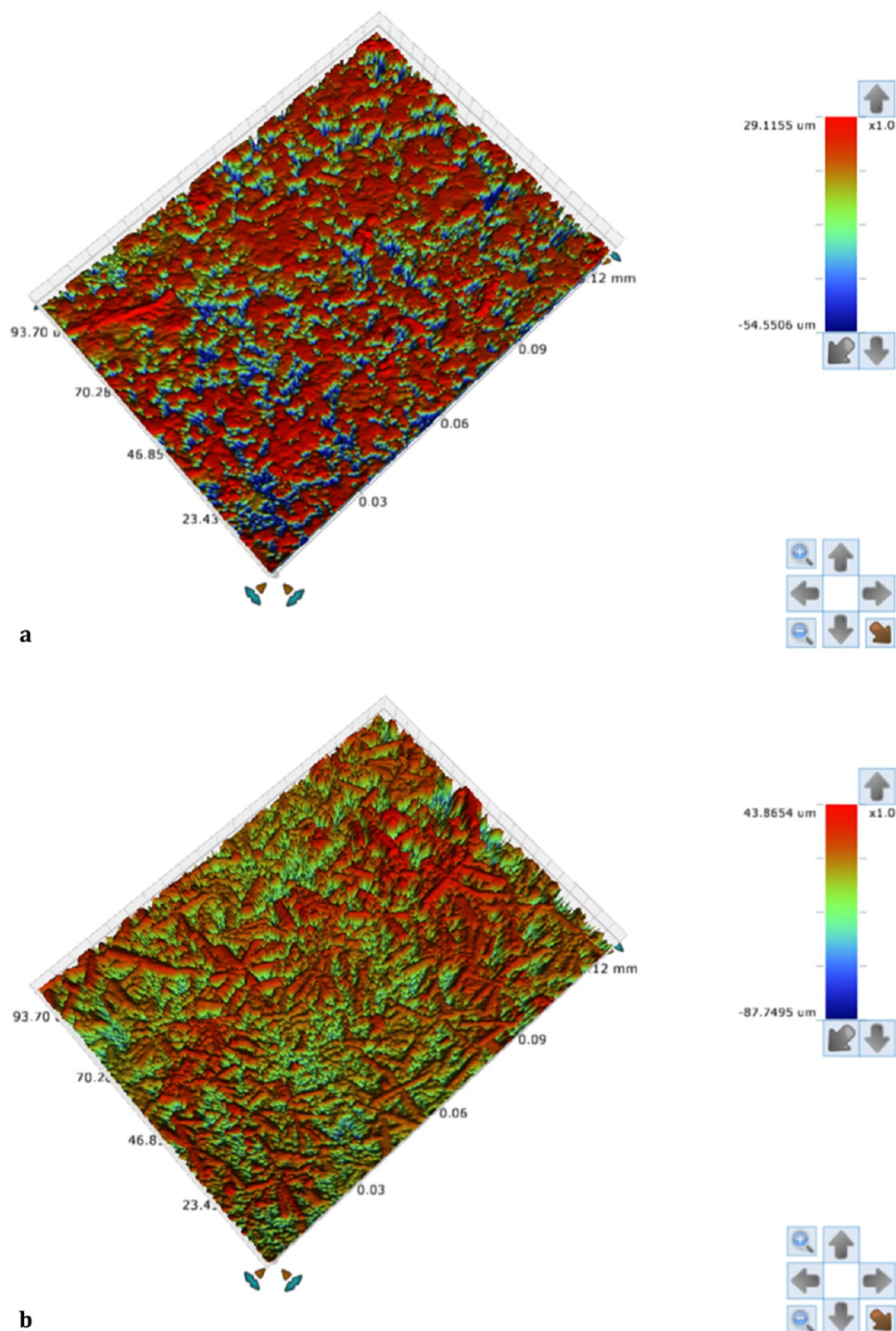


Figure 3. Optical profiler images of (a) ordered FA coating and (b) disordered FA coating on SS discs.

layer covering the titanium implants in comparison to 40% integration in the case of the disordered FA coating.³⁷ Therefore, ordered FA coatings similar to those in the present study exhibit good hard tissue compatibility *in vivo*. Although they promote osseointegration, HA implant coatings have demonstrated dubious longevity because of high dissolution

rates *in situ*.³⁸ With FA, replacement of hydroxide ions with fluoride creates a more-stable and less-soluble structure. Several authors have reported significantly less dissolution and degradation rates in FA implant coatings compared with HA.^{19,21,24,39}

Table 4. Zeta Potential Measurements of FA Powder and the Various Bacterial Strains in 0.01 M PBS and in the Presence of BHI

sample	ζ (mV) in 0.01 M PBS	Z (mV) BHI
FA powder	-1.55 ± 1.31	-0.03 ± 0.02
<i>P. gingivalis</i>	-27.89 ± 0.76	-9.60 ± 0.62
<i>F. nucleatum</i>	-37.20 ± 1.82	-15.83 ± 0.68
<i>A. actinomycetemcomitans</i>	-12.68 ± 1.82	-2.92 ± 0.53

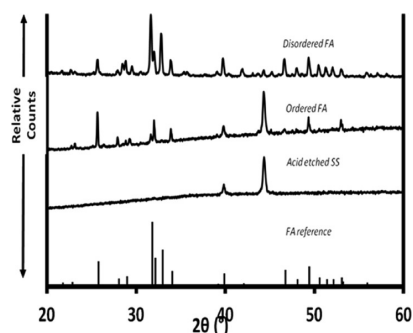


Figure 4. XRD patterns of the substrate and coatings compared with a reference FA standard.

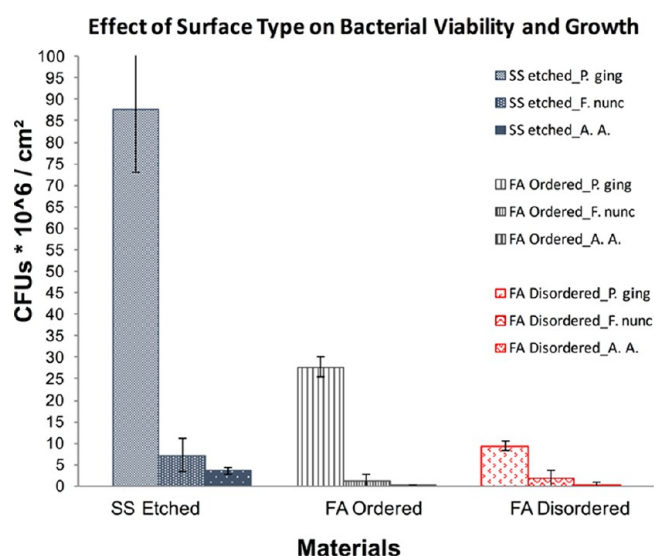


Figure 5. Effect of substrate on the retention and viability of *P. gingivalis*, *F. nucleatum*, and *A. actinomycetemcomitans*, as quantified by the CFUs counting method 48 h post adhesion (the FA coatings significantly reduced the bacterial growth in comparison to the control $p < 0.05$).

In addition to the current research on the osteointegration capabilities of a surface-coated implant, there has been a growing interest in the long-term maintenance of the marginal alveolar bone and soft tissue health. It has been well established that the bone and the soft tissue interface around the dental implants are strongly associated with each other.^{40,41} There remains a strong consensus among dental implant clinicians that hard and soft tissues must remain healthy to ensure the longevity of the implant. The soft tissues that seal around the transmucosal element of the dental implant is considered to be a vital barrier to preventing the onset of peri-mucositis. In a recent paper by De Wilde et al., nano HA coatings applied in the transmucosal element of the dental implants have

demonstrated no increase in inflammation, when compared with noncoated transmucosal abutments.⁴²

The growth of human gingival fibroblast (HGF) on FA surfaces showed that FA supports the growth and proliferation of HGFs. In particular, there was no significant difference between the number of HGF grown on the control (SS) and FA surfaces at day 1, 3, and 14, supporting the biocompatibility of FA coatings around the oral soft tissues.⁴³

4.2. Antibacterial Efficacy. The CFU data shows that all three bacteria had significantly less growth ($p \leq 0.05$) on the disordered and ordered FA coatings when compared with the acid-etched SS discs. In addition, the CLSM images illustrate fewer dead bacteria found on the SS discs, suggesting increased bactericidal activity in the FA coatings. It can thus be inferred that the FA coatings produced by the hydrothermal method significantly reduce the viability of these particular periodontal pathogens. There are several possible explanations for the results.

4.2.1. Fluoride Ions. Fluoride is known to affect the metabolism and growth of oral bacteria through a variety of complex indirect mechanisms. The weak-acid character of fluoride alters the membrane permeability to protons and compromises F-ATPase molecules, which would normally regulate a proton gradient.^{23,44} Acidification of the cytoplasm follows, which results in glycolytic enzyme inhibition, reduced cellular uptake and secretion, and a lowered aciduricity.⁴⁴ For these reasons, many authors consider the weak-acid character of fluoride to be its dominating antibacterial property.²³

Fluoride also exhibits direct antimicrobial action, binding and inhibiting a number of metabolic enzymes. These include enolase, ATP-synthase, and a number of oxidative and metallo-enzymes.^{44–46} The production of intracellular and extracellular polysaccharides, such as glucan, is reduced as a consequence.⁴⁷ Deactivating enolase blocks both the Embden–Meyerhof–Parnas (EMP) pathway and phosphor-transferase system, by halting phosphoenolpyruvate (PEP) production.⁴⁴ By preventing these particular metabolic pathways, fluoride reduces the plaque acid synthesis as well.

Collectively, the indirect and direct actions of fluoride on bacteria lead to restricted metabolism and inhibited growth and may even cause cell death.²³ Looking at the data in Table 1, the EDS and fluoride electrode analyses (as expected) identified a significantly higher fluoride content and release in both FA coatings than in the SS discs. It is therefore reasonable to assume that the presence of fluoride in the FA coatings played a role in reducing the growth of all three bacteria tested, compared with the etched SS where there were only trace amounts. This is corroborated by Ge et al. (2010), who observed less growth of *P. gingivalis* on fluoridated HA compared with titanium and HA alone.²⁷ However, in a recent study by Zhao et al. (2016), the antibacterial activity of fluorinated HA against *Staphylococcus aureus* was found to be very limited.²⁶ The difference in the antibacterial potential of fluoride against various bacterial species indicates that FA coatings would have greater efficacy against pathogens implicated in peri-implantitis rather than against bone infections where Staphylococcal species are more prominent and where silver-containing apatites are reported to be more effective.^{26,48}

4.2.2. Surface Properties. It is generally believed that the physicochemical properties of an implant coating may have a contributory effect on the bacterial adhesion and growth.^{49,50}

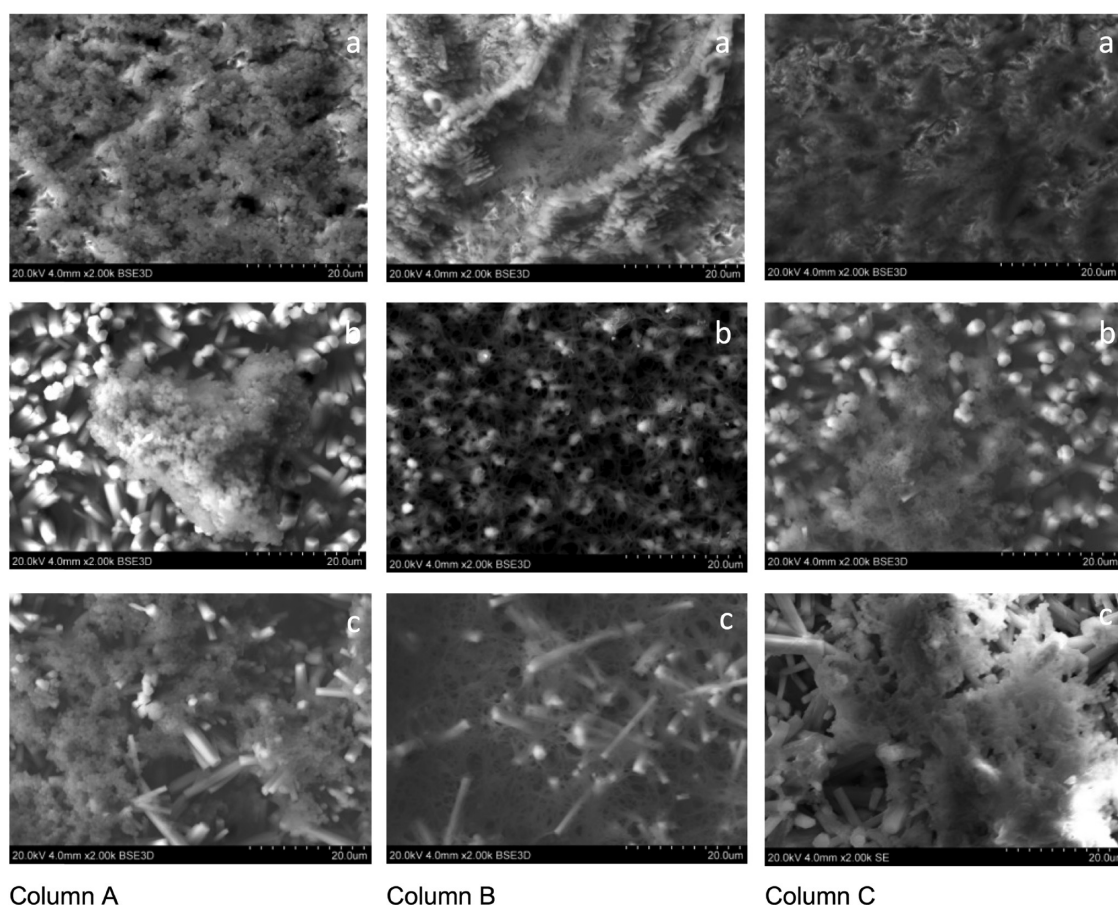


Figure 6. Column A shows the SEM images of *P. gingivalis* on (a) SS, (b) ordered, and (c) disordered FA coatings, 48 h post adhesion. Column B shows the SEM images of *F. nucleatum* on (a) SS, (b) ordered, and (c) disordered FA coatings, 48 h post adhesion. Column C shows the SEM images of *A. actinomycetemcomitans* on (a) SS, (b) ordered, and (c) disordered FA coatings, 48 h post adhesion.

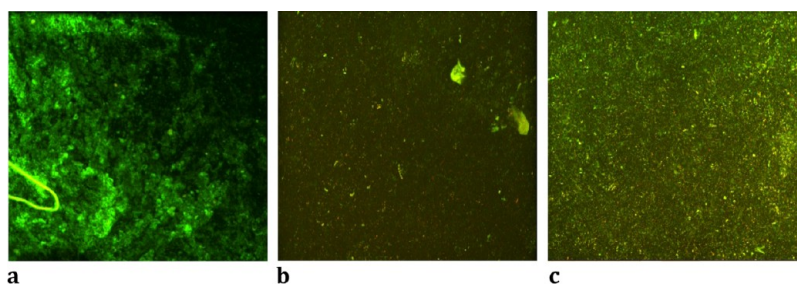


Figure 7. CLSM images of *P. gingivalis* on (a) SS, (b) ordered, and (c) disordered FA coatings, 48 h post adhesion (green: live bacteria, red: dead bacteria).

Table 3 illustrates that the surface roughness values (S_a/S_z) of the disordered FA discs are significantly higher than those of the other discs. This is due to the disordered FA coating having a thicker and uneven thickness of FA crystals on the substrate. Supragingival biofilm accumulation is generally more on a rougher surface, but no difference has been observed subgingivally⁵¹ and on varied implant surfaces.^{52,53} Furthermore, Jeyachandran et al. (2007) concluded that surface roughness was a less important factor in influencing bacterial adhesion to a coating, when compared with its chemical composition.²⁸

The surface charge of biomaterials has been proven to affect the level of bacterial adhesion because of the inherent net negative surface charge of most microbes⁵⁴ and as confirmed for the pathogens examined in this study (Table 4). A number

of authors have observed lower bacterial adhesion on negatively charged surfaces because of a degree of electrostatic repulsion.^{55,56} The zeta potential measurements illustrated in Table 3 show that the SS discs exhibit a significantly more negative surface charge than do both FA coatings whereas the disordered FA coating appears almost neutral. Despite this, by the end of the study, significantly more CFUs of all three bacteria samples were found on the SS discs. Gottenbos et al. had similar results, reporting a subset of negatively charged bacilli to adhere less yet exhibit increased growth on negatively charged surfaces.⁵⁵ Therefore, it is plausible that the electrostatic interactions had a lesser influence on the eventual colonization of the disc surfaces, compared with other reported variables such as the fluoride content and the surface roughness.

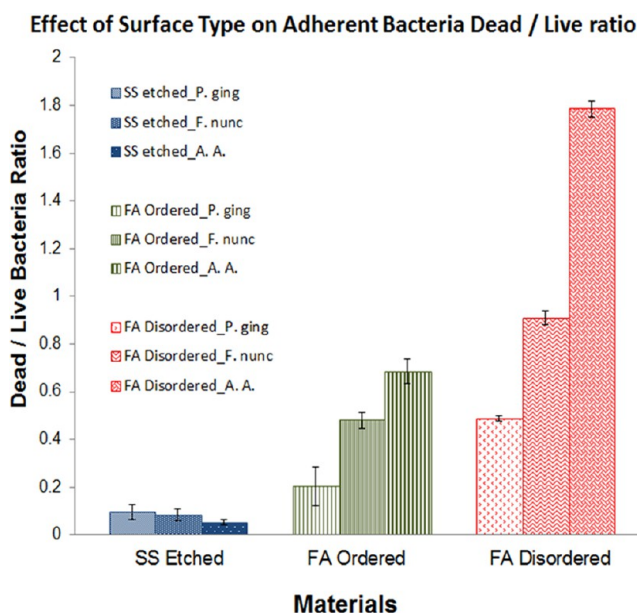


Figure 8. Effect of the surface type on adherent live/dead ratio of the bacteria as evaluated by the CLSM images analysis, 48 h post adhesion.

The process of bacterial adhesion to the underlying surface is multifactorial. Various surface characteristics such as fluoride content, surface roughness, surface wettability, and surface charge cumulatively play a role in bacterial adhesion and cellular death. The CFUs count of both *F. nucleatum* and *A. actinomycetemcomitans* were lower on the ordered FA coatings compared with the disordered FA, despite the latter exhibiting a significantly higher fluoride release (Table 1). This could be attributed to the greater negative surface charge of the ordered FA, leading to electrostatic repulsion and reduced adhesion of these two species. The CFUs count of *P. gingivalis* has been found to be lower on the disordered FA-coated discs even though this surface appeared neutral. The increased material surface wettability has been suggested as one way to reduce bacterial adhesion to material surfaces.⁴⁹ The decrease in bacterial adhesion to ordered FA could therefore be partially attributed to its higher wettability in comparison to the bare SS. The porosity of the disordered FA contributed to the increase in surface wettability, complicating the possible correlation between bacterial adhesion and surface wettability. Microbial species have been found to vary in sensitivity to the antibacterial actions of fluoride, which could explain this result.⁵⁷ Indeed, the CLSM images illustrate that more dead bacteria were found on the disordered FA; combined with the CFUs counting results, it is reasonable to assume that *P. gingivalis* makes up a significant proportion of the dead bacteria imaged. However, this could partly be due to the neutral surface charge and increased surface roughness of the disordered FA attracting more bacteria to be killed from the outset. Therefore, it cannot be concluded that the disordered FA exhibits greater inherent bactericidal properties than the ordered FA. In addition, a great number of bacteria remained attached to the disordered FA coating as observed by the SEM, and most of these appeared to be dead as confirmed by the CFUs and confocal imaging and analysis. The presence of bacteria, even if these are dead, can inhibit osseointegration,⁵⁸ showing that the ordered FA coating is a more promising dental coating than the disordered one, even though they both show similar reduction

in bacterial growth, more than 80%, when compared with the SS.

The novel FA coatings produced in the present study show resounding antimicrobial properties against all three pathogens involved, which are strongly implicated in peri-implantitis. Several alternative implant materials and coatings have been developed in the past to prevent the surface colonization and onset of peri-implantitis. However, their success has been limited.

Various titanium surface modifications have been trialed. Incorporating surface micro-/nanofeatures could downregulate inflammatory events,⁵⁹ but no effect on bacterial colonization has been observed.⁶⁰ Anodization, ion implantation, and ion plating have only been shown to modify, and not reduce, the biofilm formation.^{61,62}

HA coatings have produced conflicting results. Some antimicrobial activity has been found,¹³ particularly when imbued with metal ions like silver.^{63–67} Other authors dispute this, citing no reduction in plaque maturation^{68,69} or disease progression.⁷⁰ Indeed, increased bone loss has been observed around HA-coated implants in the presence of infection.^{71–73} Incorporating antimicrobial agents into HA may provide temporary benefit, but its long-term use is not proved and uncertain.^{12,74}

Overall, the fluoride content, rather than its release, is likely to be the most influential variable in reducing the count and viability of the bacteria tested. However, as seen with the ordered FA, surface characteristics may also have some impact on the results. It would be useful to identify the ideal fluoride concentration, in relation to surface charge, that confers superior antibacterial activity against a broader range of periodontopathogens such as *Prevotella intermedia* and *Bacteroides forsythus*.⁷⁵ Incorporating titanium as the substrate in these further investigations would enhance the clinical relevance to implant usage. Investigating the degradation and dissolution rates of these novel FA coatings is vital, despite other fluoride-containing apatites exhibiting good stability.⁷⁶ Kim et al. (2003) showed that the FA composites did not show any signs of host cytotoxicity whereas the fluoride actually had a stimulating effect on cell proliferation and alkaline phosphatase (ALP) activities.⁷⁷

5. CONCLUSION

These promising results indicate that FA produced using a hydrothermal process may be used as a dental implant coating that shows significant antibacterial activity against bacteria implicated in peri-implantitis.

However, the results also reflect the need to optimize the level of fluoride in the FA coating to have optimum antibacterial efficacy without compromising the stability and resistance to the dissolution of the coating.

■ ASSOCIATED CONTENT

📄 Supporting Information

The Supporting Information is available free of charge on the ACS Publications website at DOI: 10.1021/acsomega.6b00080.

SEM images of FA crystals on both titanium and SS substrates (PDF)

AUTHOR INFORMATION

Corresponding Authors

*E-mail: d.j.wood@leeds.ac.uk. Phone: +44(0)113 343 6192 (D.J.W.).

*E-mail: m.katsikogianni@bradford.ac.uk. Phone: +44(0)127 423 3741 (M.G.K.).

Author Contributions

The manuscript was written through contributions of all authors. All authors have given approval to the final version of the manuscript.

Notes

The authors declare no competing financial interest.

ACKNOWLEDGMENTS

The authors wish to thank Jackie Hudson for her help with the CLSM and SEM, Dr. William Vickers for the XRD analysis, and Shabnum Rashid for her assistance in microbiology. The National EPSRC XPS Users' Service (NEXUS) and Dr. Matthew German are acknowledged for their assistance with the XPS analysis. This work was partially funded through WELMEC, a Centre of Excellence in Medical Engineering funded by the Wellcome Trust and EPSRC, under grant number WT 088908/Z/09/Z.

REFERENCES

- (1) Jung, R. E.; Pjetursson, B. E.; Glauser, R.; Zembic, A.; Zwahlen, M.; Lang, N. P. A systematic review of the 5-year survival and complication rates of implant-supported single crowns. *Clin. Oral Implants Res.* **2008**, *19*, 119–130.
- (2) Charyeva, O.; Altynbekov, K.; Zhartybaev, R.; Sabdanaliev, A. Long-term dental implant success and survival—a clinical study after an observation period up to 6 years. *Swed. Dent. J.* **2012**, *36*, 1–6.
- (3) Simonis, P.; Dufour, T.; Tenenbaum, H. Long-term implant survival and success: A 10–16-year follow-up of non-submerged dental implants. *Clin. Oral Implants Res.* **2010**, *21*, 772–777.
- (4) Michelinakis, G.; Sharrock, A.; Barclay, C. W. Identification of dental implants through the use of implant recognition software (IRS). *Int. Dent. J.* **2006**, *56*, 203–208.
- (5) Han, H.-J.; Kim, S.; Han, D.-H. Multifactorial evaluation of implant failure: A 19-year retrospective study. *Int. J. Oral Maxillofac. Implants* **2014**, *29*, 303–310.
- (6) Atieh, M. A.; Alsabeeha, N. H. M.; Faggion, C. M., Jr.; Duncan, W. J. The frequency of peri-implant diseases: A systematic review and meta-analysis. *J. Periodontol.* **2013**, *84*, 1586–1598.
- (7) Klinge, B.; Meyle, J.; Working Group 2. Peri-Implant Tissue Destruction. The Third EAO Consensus Conference 2012. *Clin. Oral Implants Res.* **2012**, *23*, 108–110.
- (8) Esposito, M.; Grusovin, M. G.; Worthington, H. V. Treatment of peri-implantitis: What interventions are effective? A Cochrane systematic review. *Eur. J. Oral Implantol.* **2012**, *5*, S21–S41.
- (9) Tamura, N.; Ochi, M.; Miyakawa, H.; Nakazawa, F. Analysis of bacterial flora associated with peri-implantitis using obligate anaerobic culture technique and 16S rDNA gene sequence. *Int. J. Oral Maxillofac. Implants* **2013**, *28*, 1521–1529.
- (10) Persson, G. R.; Renvert, S. Cluster of Bacteria Associated with Peri-Implantitis. *Clin. Implant Dent. Relat. Res.* **2014**, *16*, 783–793.
- (11) Schmalz, G.; Tsigaras, S.; Rinke, S.; Kottmann, T.; Haak, R.; Ziebolz, D. Detection of five potentially periodontal pathogenic bacteria in peri-implant disease: A comparison of PCR and real-time PCR. *Diagn. Microbiol. Infect. Dis.* **2016**, *85*, 289–294.
- (12) Montanaro, L.; Campoccia, D.; Arciola, C. R. Advancements in molecular epidemiology of implant infections and future perspectives. *Biomaterials* **2007**, *28*, 5155–5168.
- (13) Mathew, D.; Bardwaj, G.; Wang, Q.; Sun, L.; Ercan, B.; Manisavagam, G.; Webster, T. J. Decreased *Staphylococcus aureus* and increased osteoblast density on nanostructured electrophoretic

deposited hydroxyapatite on titanium without the use of pharmaceuticals. *Int. J. Nanomed.* **2014**, *9*, 1775–1781.

- (14) Oonishi, H.; Yamamoto, M.; Ishimaru, H.; Tsuji, E.; Kushitani, S.; Aono, M.; Ukon, Y. The effect of hydroxyapatite coating on bone growth into porous titanium alloy implants. *J. Bone Jt. Surg., Br. Vol.* **1989**, *71*, 213–216.

- (15) Shi, J.; Dong, L. L.; He, F.; Zhao, S.; Yang, G.-L. Osteoblast responses to thin nanohydroxyapatite coated on roughened titanium surfaces deposited by an electrochemical process. *Oral Surg., Oral Med., Oral Pathol.* **2013**, *116*, e311–e316.

- (16) Alsabeeha, N. H.; Ma, S.; Atieh, M. A. Hydroxyapatite-coated oral implants: A systematic review and meta-analysis. *Int. J. Oral Maxillofac. Implants* **2012**, *27*, 1123–1130.

- (17) Chen, H.; Tang, Z.; Liu, J.; Sun, K.; Chang, S.-R.; Peters, M. C.; Mansfield, J. F.; Czajka-Jakubowska, A.; Clarkson, B. H. Acellular synthesis of a human enamel-like microstructure. *Adv. Mater.* **2006**, *18*, 1846.

- (18) Cheng, K.; Weng, W.; Wang, H.; Zhang, S. In vitro behavior of osteoblast-like cells on fluoridated hydroxyapatite coatings. *Biomaterials* **2005**, *26*, 6288–6295.

- (19) Wang, Y.; Zhang, S.; Zeng, X.; Ma, L. L.; Weng, W.; Yan, W.; Qian, M. Osteoblastic cell response on fluoridated hydroxyapatite coatings. *Acta Biomater.* **2007**, *3*, 191–197.

- (20) Liu, J.; Jin, T.; Chang, S.; Czajka-Jakubowska, A.; Zhang, Z.; Nör, J. E.; Clarkson, B. H. The effect of novel fluorapatite surfaces on osteoblast-like cell adhesion, growth, and mineralization. *Tissue Eng., Part A* **2010**, *16*, 2977–2986.

- (21) Bhadang, K. A.; Gross, K. A. Influence of fluorapatite on the properties of thermally sprayed hydroxyapatite coatings. *Biomaterials* **2004**, *25*, 4935–4945.

- (22) Ohno, M.; Kimoto, K.; Toyoda, T.; Kawata, K.; Arakawa, H. Fluoride-treated bio-resorbable synthetic hydroxyapatite promotes proliferation and differentiation of human osteoblastic MG-63 cells. *J. Oral Implantol.* **2013**, *39*, 154–160.

- (23) Marquis, R. E. Antimicrobial actions of fluoride for oral bacteria. *Can. J. Microbiol.* **1995**, *41*, 955–964.

- (24) Dhert, W. J. A.; Klein, C. P. A. T.; Jansen, J. A.; van der Velde, E. A.; Vriesde, R. C.; Rozing, P. M.; de Groot, K. A histological and histomorphometrical investigation of fluorapatite, magnesiumwhitlockite, and hydroxylapatite plasma-sprayed coatings in goats. *J. Biomed. Mater. Res.* **1993**, *27*, 127–138.

- (25) Avila, G.; Misch, K.; Galindo-Moreno, P.; Wang, H.-L. Implant surface treatment using biomimetic agents. *Implant Dent.* **2009**, *18*, 17–26.

- (26) Zhao, C.; Hou, P.; Ni, J.; Han, P.; Chai, Y.; Zhang, X. Ag-Incorporated FHA Coating on Pure Mg: Degradation and In Vitro Antibacterial Properties. *ACS Appl. Mater. Interfaces* **2016**, *8*, 5093–5103.

- (27) Ge, X.; Leng, Y.; Bao, C.; Xu, S. L.; Wang, R.; Ren, F. Antibacterial coatings of fluoridated hydroxyapatite for percutaneous implants. *J. Biomed. Mater. Res., Part A* **2010**, *95*, 588–599.

- (28) Jeyachandran, Y. L.; Venkatachalam, S.; Karunakaran, B.; Narayandass, S. K.; Mangalaraj, D.; Bao, C. Y.; Zhang, C. L. Bacterial adhesion studies on titanium, titanium nitride and modified hydroxyapatite thin films. *Mater. Sci. Eng. C* **2007**, *27*, 35–41.

- (29) Hoover, C. I.; Newbrun, E. Survival of Bacteria from Human Dental Plaque Under Various Transport Conditions. *J. Clin. Microbiol.* **1977**, *6*, 212–218.

- (30) Chen, H.; Tang, Z.; Liu, J.; Sun, K.; Chang, S.-R.; Peters, M. C.; Mansfield, J. F.; Czajka-Jakubowska, A.; Clarkson, B. H. Acellular Synthesis of a Human Enamel-like Microstructure. *Adv. Mater.* **2006**, *18*, 1846–1851.

- (31) Czajka-Jakubowska, A. E.; Liu, J.; Chang, S. R.; Clarkson, B. H. The effect of the surface characteristics of various substrates on fluorapatite crystal growth, alignment, and spatial orientation. *Med. Sci. Monit.* **2009**, *15*, MT84–8.

- (32) Okazaki, M.; Moriwaki, Y.; Aoba, T.; Doi, Y.; Takahashi, J. Solubility behavior of CO₃ apatites in relation to crystallinity. *Caries Res.* **1981**, *15*, 477–483.

- (33) Chen, H.; Czajka-Jakubowska, A.; Spencer, N. J.; Mansfield, J. F.; Robinson, C.; Clarkson, B. H. Effects of systemic fluoride and in vitro fluoride treatment on enamel crystals. *J. Dent. Res.* **2006**, *85*, 1042–1045.
- (34) Kim, H.-W.; Kim, H.-E.; Knowles, J. C. Fluor-hydroxyapatite sol–gel coating on titanium substrate for hard tissue implants. *Biomaterials* **2004**, *25*, 3351–3358.
- (35) Cheng, K.; Weng, W.; Qu, H.; Du, P.; Shen, G.; Han, G.; Yang, J.; Ferreira, J. M. F. Sol-gel preparation and in vitro test of fluorapatite/hydroxyapatite films. *J. Biomed. Mater. Res., Part B* **2004**, *69*, 33–37.
- (36) Sakae, T.; Hoshino, K.; Fujimori, Y.; Kozawa, Y.; LeGeros, R. Z. In vitro interactions of bone marrow cells with carbonate and fluoride containing apatites. *Key Eng. Mater.* **2001**, *192*, 347–350.
- (37) Liu, J.; Jin, T.; Chang, S.; Czajka-Jakubowska, A.; Zhang, Z.; Nör, J. E.; Clarkson, B. H. The effect of novel fluorapatite surfaces on osteoblast-like cell adhesion, growth, and mineralization. *Tissue Eng., Part A* **2010**, *16*, 2977–2986.
- (38) Avila, G.; Misch, K.; Galindo-Moreno, P.; Wang, H.-L. Implant surface treatment using biomimetic agents. *Implant Dent.* **2009**, *18*, 17–26.
- (39) Cheng, K.; Weng, W.; Qu, H.; Du, P.; Shen, G.; Han, G.; Yang, J.; Ferreira, J. M. F. Sol-gel preparation and in vitro test of fluorapatite/hydroxyapatite films. *J. Biomed. Mater. Res., Part B* **2004**, *69*, 33–37.
- (40) Vandeweghe, S.; De Bruyn, H. A within-implant comparison to evaluate the concept of platform switching: A randomised controlled trial. *Eur. J. Oral Implantol.* **2012**, *5*, 253–262.
- (41) Romanos, G. E.; Traini, T.; Johansson, C. B.; Piattelli, A. Biologic width and morphologic characteristics of soft tissues around immediately loaded implants: Studies performed on human autopsy specimens. *J. Periodontol.* **2010**, *81*, 70–78.
- (42) De Wilde, E. A. W. J.; Jimbo, R.; Wennerberg, A.; Naito, Y.; Coucke, P.; Bryington, M. S.; Vandeweghe, S.; De Bruyn, H. The soft tissue immunologic response to hydroxyapatite-coated transmucosal implant surfaces: A study in humans. *Clin. Implant Dent. Relat. Res.* **2015**, *17*, e65–e74.
- (43) Clarkson, B. H.; Scott, T. F. Bioactive “smart” dental composite materials. WO2015143258 A1, Sept 24, 2015.
- (44) Marsh, P. *Oral Microbiology*, 4th ed.; Reed Educational and Professional Publishing Ltd., 1999.
- (45) Vogel, G. L.; Zhang, Z.; Chow, L. C.; Schumacher, G. E. Changes in lactate and other ions in plaque and saliva after a fluoride rinse and subsequent sucrose administration. *Caries Res.* **2002**, *36*, 44–52.
- (46) Takahashi, N.; Washio, J. Metabolomic Effects of Xylitol and Fluoride on Plaque Biofilm In Vivo. *J. Dent. Res.* **2011**, *90*, 1463–1468.
- (47) Koo, H.; Sheng, J.; Nguyen, P. T. M.; Marquis, R. E. Co-operative inhibition by fluoride and zinc of glucosyl transferase production and polysaccharide synthesis by mutans streptococci in suspension cultures and biofilms. *FEMS Microbiol. Lett.* **2006**, *254*, 134–140.
- (48) Lim, P. N.; Chang, L.; Tay, B. Y.; Guneta, V.; Choong, C.; Ho, B.; Thian, E. S. Proposed mechanism of antibacterial action of chemically modified apatite for reduced bone infection. *ACS Appl. Mater. Interfaces* **2014**, *6*, 17082–17092.
- (49) Katsikogianni, M. G.; Wood, D. J.; Missirlis, Y. F. Biomaterial Functionalized Surfaces for Reducing Bacterial Adhesion and Infection; In *Handbook of Bioceramics and Biocomposites*; Antoniac, I. V., Ed.; Springer International Publishing: Cham, 2016; pp 1–28.
- (50) Katsikogianni, M.; Missirlis, Y. F. Concise review of mechanisms of bacterial adhesion to biomaterials and of techniques used in estimating bacteria-material interactions. *Eur. Cells Mater.* **2004**, *8*, 37–57.
- (51) Elter, C.; Heuer, W.; Demling, A.; Hannig, M.; Heidenblut, T.; Bach, F. W.; Stiesch-Scholz, M. Supra- and subgingival biofilm formation on implant abutments with different surface characteristics. *Int. J. Oral Maxillofac. Implants* **2008**, *23*, 327–334.
- (52) Lin, H. Y.; Liu, Y.; Wismeijer, D.; Crielaard, W.; Deng, D. M. Effects of oral implant surface roughness on bacterial biofilm formation and treatment efficacy. *Int. J. Oral Maxillofac. Implants* **2013**, *28*, 1226–1231.
- (53) Quirynen, M.; Van Der Mei, H. C.; Bollen, C. M. L.; Schotte, A.; Marechal, M.; Doornbusch, G. I.; Naert, I.; Busscher, H. J.; Van Steenberghe, D. An in vivo study of the influence of the surface roughness of implants on the microbiology of supra- and subgingival plaque. *J. Dent. Res.* **1993**, *72*, 1304–1309.
- (54) Wilson, W. W.; Wade, M. M.; Holman, S. C.; Champlin, F. R. Status of methods for assessing bacterial cell surface charge properties based on zeta potential measurements. *J. Microbiol. Methods* **2001**, *43*, 153–164.
- (55) Gottenbos, B.; Grijpma, D. W.; van der Mei, H. C.; Feijen, J.; Busscher, H. J. Antimicrobial effects of positively charged surfaces on adhering Gram-positive and Gram-negative bacteria. *J. Antimicrob. Chemother.* **2001**, *48*, 7–13.
- (56) Weerkamp, A. H.; Uyen, H. M.; Busscher, H. J. Effect of zeta potential and surface energy on bacterial adhesion to uncoated and saliva-coated human enamel and dentin. *J. Dent. Res.* **1988**, *67*, 1483–1487.
- (57) Li, Y. H.; Bowden, G. H. The effect of environmental pH and fluoride from the substratum on the development of biofilms of selected oral bacteria. *J. Dent. Res.* **1994**, *73*, 1615–1626.
- (58) Wei, T.; Yu, Q.; Zhan, W.; Chen, H. Antibacterial Surfaces: A Smart Antibacterial Surface for the On-Demand Killing and Releasing of Bacteria. *Adv. Healthcare Mater.* **2016**, *5*, 396.
- (59) Palmquist, A.; Johansson, A.; Suska, F.; Brånemark, R.; Thomsen, P. Acute inflammatory response to laser-induced micro- and nano-sized titanium surface features. *Clin. Implant Dent. Relat. Res.* **2013**, *15*, 96–104.
- (60) Fröjd, V.; Linderbäck, P.; Wennerberg, A.; de Paz, L. C.; Svensäter, G.; Davies, J. R. Effect of nanoporous TiO₂ coating and anodized Ca²⁺ modification of titanium surfaces on early microbial biofilm formation. *BMC Oral Health* **2011**, *11*, 8.
- (61) Caous, J. S.; Lövenklev, M.; Fäldt, J.; Langton, M. Adhesion of *Streptococcus mitis* and *Actinomyces oris* in co-culture to machined and anodized titanium surfaces as affected by atmosphere and pH. *BMC Oral Health* **2013**, *13*, 4.
- (62) Yoshinari, M.; Oda, Y.; Kato, T.; Okuda, K.; Hirayama, A. Influence of surface modifications to titanium on oral bacterial adhesion in vitro. *J. Biomed. Mater. Res.* **2000**, *52*, 388–394.
- (63) Ghani, Y.; Coathup, M. J.; Hing, K. A.; Blunn, G. W. Development of a hydroxyapatite coating containing silver for the prevention of peri-prosthetic infection. *J. Orthop. Res.* **2012**, *30*, 356–363.
- (64) Lim, P. N.; Shi, Z.; Neoh, K. G.; Ho, B.; Tay, B. Y.; Thian, E. S. The effects of silver, silicon-containing apatite towards bacteria and cell responses. *Biomed. Mater.* **2014**, *9*, 015010.
- (65) O’Sullivan, C.; O’Hare, P.; O’Leary, N. D.; Crean, A. M.; Ryan, K.; Dobson, A. D. W.; O’Neill, L. Deposition of substituted apatites with anticolonizing properties onto titanium surfaces using a novel blasting process. *J. Biomed. Mater. Res., Part B* **2010**, *95*, 141–149.
- (66) Roy, M.; Fielding, G. A.; Beyenal, H.; Bandyopadhyay, A.; Bose, S. Mechanical, in vitro antimicrobial, and biological properties of plasma-sprayed silver-doped hydroxyapatite coating. *ACS Appl. Mater. Interfaces* **2012**, *4*, 1341–1349.
- (67) Thian, E. S.; Konishi, T.; Kawanobe, Y.; Lim, P. N.; Choong, C.; Ho, B.; Aizawa, M. Zinc-substituted hydroxyapatite: A biomaterial with enhanced bioactivity and antibacterial properties. *J. Mater. Sci.: Mater. Med.* **2013**, *24*, 437–445.
- (68) Yamane, K.; Ayukawa, Y.; Takeshita, T.; Furuhashi, A.; Yamashita, Y.; Koyano, K. Bacterial adhesion affinities of various implant abutment materials. *Clin. Oral Implants Res.* **2013**, *24*, 1310–1315.
- (69) Gatewood, R. R.; Cobb, C. M.; Killoy, W. J. Microbial colonization on natural tooth structure compared with smooth and plasma-sprayed dental implant surfaces. *Clin. Oral Implants Res.* **1993**, *4*, 53–64.
- (70) Madi, M.; Zakari, O.; Noritake, K.; Fuji, M.; Kasugai, S. Peri-implantitis progression around thin sputtered hydroxyapatite-coated

implants: Clinical and radiographic evaluation in dogs. *Int. J. Oral Maxillofac. Implants* **2013**, *28*, 701–709.

(71) Oosterbos, C. J. M.; Vogely, H. C.; Nijhof, M. W.; Fleer, A.; Verbout, A. J.; Tonino, A. J.; Dhert, W. J. A. Osseointegration of hydroxyapatite-coated and noncoated Ti6Al4V implants in the presence of local infection: A comparative histomorphometrical study in rabbits. *J. Biomed. Mater. Res.* **2002**, *60*, 339–347.

(72) Jovanovic, S. A.; Kenney, E. B.; Carranza, F. A., Jr.; Donath, K. The regenerative potential of plaque-induced peri-implant bone defects treated by a submerged membrane technique: An experimental study. *Int. J. Oral Maxillofac. Implants* **1993**, *8*, 13–18.

(73) Gottlander, M.; Johansson, C. B.; Albrektsson, T. Short- and long-term animal studies with a plasma-sprayed calcium phosphate-coated implant. *Clin. Oral Implants Res.* **1997**, *8*, 345–351.

(74) Norowski, P. A., Jr.; Bumgardner, J. D. Biomaterial and antibiotic strategies for peri-implantitis: A review. *J. Biomed. Mater. Res., Part B* **2009**, *88*, 530–543.

(75) Hultin, M.; Gustafsson, A.; Hallstrom, H.; Johansson, L.-A.; Ekfeldt, A.; Klinge, B. Microbiological findings and host response in patients with peri-implantitis. *Clin. Oral Implants Res.* **2002**, *13*, 349–358.

(76) Gineste, L.; Gineste, M.; Ranz, X.; Elleferion, A.; Guilhem, A.; Rouquet, N.; Frayssinet, P. Degradation of hydroxylapatite, fluorapatite, and fluorhydroxyapatite coatings of dental implants in dogs. *J. Biomed. Mater. Res.* **1999**, *48*, 224–234.

(77) Kim, H.-W.; Noh, Y.-J.; Koh, Y.-H.; Kim, H.-E. Enhanced performance of fluorine substituted hydroxyapatite composites for hard tissue engineering. *J. Mater. Sci.: Mater. Med.* **2003**, *14*, 899–904.